The Journal of Immunology

Matrix Architecture Dictates Three-Dimensional Migration Modes of Human Macrophages: Differential Involvement of Proteases and Podosome-Like Structures

Emeline Van Goethem, Renaud Poincloux, Fabienne Gauffre, Isabelle Maridonneau-Parini and Véronique Le Cabec

J Immunol 2010; 184:1049-1061; Prepublished online 16 December 2009;
doi: 10.4049/jimmunol.0902223
http://www.jimmunol.org/content/184/2/1049

The Journal of Immunology is published twice each month by
The American Association of Immunologists, Inc.,
1451 Rockville Pike, Suite 650, Rockville, MD 20852

Print ISSN: 0022-1767 Online ISSN: 1550-6606.

Matrix Architecture Dictates Three-Dimensional Migration Modes of Human Macrophages: Differential Involvement of Proteases and Podosome-Like Structures

Emeline Van Goethem,*,† Renaud Poincloux,*,†,‡,§ Fabienne Gauffre,¶ Isabelle Maridonneau-Parini,*,† and Véronique Le Cabec*,†

Tissue infiltration of macrophages, although critical for innate immunity, is also involved in pathologies, such as chronic inflammation and cancer. In vivo, macrophages migrate mostly in a constrained three-dimensional (3D) environment. However, in vitro studies, mainly focused on two dimensions, do not provide meaningful clues about the mechanisms involved in 3D macrophage migration. In contrast, tumor cell 3D migration is well documented. It comprises a protease-independent and Rho kinase (ROCK)-dependent amoeboid migration mode and a protease-dependent and ROCK-independent mesenchymal migration mode. In this study, we examined the influence of extracellular matrix (composition, architecture, and stiffness) on 3D migration of human macrophages derived from blood monocytes (MDMs). We show that: 1) MDMs use either the amoeboid migration mode in fibrillar collagen I or the mesenchymal migration mode in Matrigel and gelled collagen I, whereas HT1080 tumor cells only perform mesenchymal migration; 2) when MDMs use the mesenchymal migratory mode, they form 3D collagenolytic structures at the tips of cell protrusions that share several markers with podosomes as described in two dimensions; 3) in contrast to tumor cells, matrix metalloproteinase inhibitors do not impair protease-dependent macrophage 3D migration, suggesting the involvement of other proteolytic systems; and 4) MDMs infiltrating matrices of similar composition but with variable stiffness adapt their migration mode primarily to the matrix architecture. In conclusion, although it is admitted that leukocytes 3D migration is restricted to the amoeboid mode, we show that human macrophages also perform the mesenchymal mode but in a distinct manner than tumor cells, and they naturally adapt their migration mode to the environmental constraints. *The Journal of Immunology*, **2010, 184: 1049–1061.**

Macrophages are present in almost all tissues of the organism where they play a central role in clearance of microorganisms, initiation and mediation of immune and inflammatory responses, and tissue repair. Nevertheless, tissue infiltration of macrophages also exacerbates pathological processes, such as chronic inflammation, neurodegenerative disorders, and cancer development (1–3). Therefore, regulation of human macrophage migration is a current therapeutic challenge (3, 4).

Extracellular matrices (ECMs) create steric barriers to cell migration. However, macrophages are able to go through most, if not all, tissues of the body. To reach tissue sites, transmigration through the endothelial wall is followed by migration through basal membranes and within interstitial tissues (see Refs. 5 and 6 for reviews). Basement membrane matrices deposited beneath epithelia and endothelia mainly contain collagen IV, laminin, perlecan, and nidogen, which form thin dense cross-linked polymeric networks with high tensile strength (7, 8). Stromal/interstitial matrices form the majority of the body connective tissue and are primarily composed of fibrillar collagen I cross-linked into a stable meshwork (8, 9). The physical structure of interstitial matrices is heterogeneous ranging from loose fibrillar regions to dense compact connective tissue with submicron spacing (3).

Although macrophage migration in two dimensions has been thoroughly studied (10, 11), the mechanisms involved in their three-dimensional (3D) infiltration into connective tissues have been poorly documented. The study of 3D macrophage migration is a critical question as two-dimensional (2D) and 3D migration appear to operate through distinct mechanisms (12, 13). 3D migration of invasive tumor cells involves two main modes with distinct characteristics: amoeboid and mesenchymal migration (9, 14–16). Amoeboid migration used by most leukocytes and tumor cells is characterized by a rounded cell shape and the lack of both strong adhesive interactions and proteolytic matrix degradation (3). Mesenchymal migration used by fibroblasts, smooth muscle cells, and also some cancer cell lines is much slower, characterized by an elongated cell shape with long membrane protrusions, the presence of strong adhesion sites and proteolytic degradation of the ECM (3). These migration modes are also distinguishable by different intracellular signaling pathways: amoeboid migration is Rho/Rho kinase (ROCK)-dependent and integrin-independent, whereas mesenchymal migration is integrin- and Src kinase-dependent but ROCK independent (15, 17–19). A shift between mesenchymal and amoeboid migration has been observed in some

*Centre National de la Recherche Scientifique and †Université de Toulouse, Université Paul Sabatier, Institut de Pharmacologie et de Biologie Structurale, Unité Mixte de Recherche 5089; ¶Laboratoire des IMRCP, Centre National de la Recherche Scientifique, Université de Toulouse, Toulouse; ‡Membrane and Cytoskeleton Dynamics, Centre National de la Recherche Scientifique, Unité Mixte de Recherche 144; and §Research Center, Institut Curie, Paris, France

Received for publication July 13, 2009. Accepted for publication November 14, 2009.

E.V.G. was supported by a fellowship from la Ligue Nationale Contre le Cancer. This work was supported in part by grants from the Association pour la Recherche Contre le Cancer (3988), the Association pour la Recherche Contre le Cancer-Institut National du Cancer for 2006, and by the Agence Nationale de la Recherce (BLAN0362).

Address correspondence and reprint requests to Dr. Isabelle Maridonneau-Parini, Institut de Pharmacologie et de Biologie Structurale, Centre National de la Recherche Scientifique, Unité Mixte de Recherche 5089, 205 Route de Narbonne, 31077 Toulouse Cedex, France. E-mail address: Isabelle.Maridonneau-parini@ipbs.fr

The online version of this article contains supplemental material.

Abbreviations used in this paper: 2D, two-dimensional; 3D, three-dimensional; ECM, extracellular matrix; HCS, high-content screening; MDM, monocyte-derived macrophage; MMP, matrix metalloproteinase; P-tyr, phosphotyrosine; PI mix, mixture of protease inhibitors; ROCK, Rho kinase.

tumor cells such as HT1080 cells when exposed to protease inhibitors (20). The "mesenchymal to amoeboid" transition involves mutually exclusive activation of Rac and Rho (21) and allows invasion in the absence of pericellular proteolysis and matrix degradation (15).

To our knowledge, the only attempt to characterize the 3D migration mode of macrophages has been performed with the macrophage cell line U937 in a collagen matrix; U937 cells proceed through a nonproteolytic and round-shape-amoeboid migration mode (22) like other leukocytes (Ref. 3 for review). The fact that proteases could be dispensable for macrophage migration is supported by a recent report showing that macrophages from matrix metalloproteinase (MMP) *Mmp9*$^{-/-}$ mice exhibit a transmatrix migration activity similar to that of wild-type cells (23) and, *in vivo*, macrophage tissue infiltration is not affected in experimental atherosclerosis performed in *Mmp13*$^{-/-}$ or *Mmp14*$^{-/-}$ (MT1-MMP) mice (24, 25) or in arterial aneurysm performed in *MT1-Mmp*$^{-/-}$ mice (26). However, other recent data indicate that proteases could be required because: 1) in vivo macrophage migration during embryonic development is MMP dependent in frog (27) and zebrafish (28); and 2) macrophages from MT1-MMP–deficient mice have a defective tissue infiltration capacity (29). Therefore, it is rather difficult to conclude what the role of proteases is in macrophage migration.

To characterize 3D migration of human macrophages, we used a simplified experimental model mimicking distinct ECM polymerized as thick layers on top of Transwell porous membranes. We show that human monocyte-derived macrophages (MDMs) are able to perform either amoeboid or mesenchymal migration and choose their migratory mode according to the biophysical parameters of the matrix.

Materials and Methods

Materials

Protease inhibitors were [L-3-*trans*-carboxyoxirane-2-carbonyl]-L-leucine (3-methylbutyl) amide (E64c; Peptide International, Lousville, KY), aprotinin (Sigma-Aldrich, St. Louis, MO), leupeptin (Sigma-Aldrich), pepstatin A (Sigma-Aldrich), and the broad-spectrum MMP inhibitor GM6001 (Calbiochem, San Diego, CA). ROCK was inhibited by the use of Y27632 (VWR International, Fontenay sous bois, France). Matrigel and BD PuraMatrix Peptide Hydrogel were purchased from BD Biosciences (San Jose, CA). Pepsin-extracted collagen I (Nutragen) was from Nutacon (Leimuiden, The Netherlands). Primary Abs were as follows: mouse anticortactin clone 4F11 and mouse antiphosphotyrosine (P-tyr) clone 4G10 (Upstate Biotechnology, Lake Placid, NY), mouse antipaxillin clone 349 (BD Transduction Laboratories, Lexington, KY), mouse antigelsolin clone GS-2C4 (Sigma-Aldrich), mouse anti-β_1 integrin clone 4B4 (Coulter clone), and rabbit polyclonal anti-COL2 3/4 C_{short} IgG (IBEX Pharmaceuticals, Montreal, Quebec, Canada).

Cell preparation and culture

Human monocytes from healthy volunteers were isolated as described previously (30). Cells were resuspended in ice-cold buffer composed of PBS, 2 mM EDTA, and 0.5% FCS at pH 7.4 and subsequently magnetically sorted by CD14 magnetic microbeads (Miltenyi Biotec, Auburn, CA). Monocytes were then distributed on glass coverslips at 1–1.5 $\times$ 10^6 in 6-well plates in RPMI 1640 without FCS to allow for their adherence. After 2 h at 37°C in humidified 5% CO_2 atmosphere, the medium was replaced by RPMI 1640 containing 10% heat-inactivated FCS, antibiotics, and 20 ng/ml M-CSF (PeproTech, Rock Hill, NJ). The cells were then maintained in culture for 6–8 d before their use. The culture medium was usually renewed on the third or fourth day of culture.

HT1080 human fibrosarcoma cells were routinely cultured and maintained in DMEM supplemented with 10% (v/v) heat-inactivated FCS, penicillin-streptomycin (100 U/ml), and L-glutamine 2 mg/ml at 37°C in humidified 5% CO_2 atmosphere.

3D matrix migration assay

Model setup. Transwell inserts with an 8-μm pore-size polyester membrane in 24-well Companion plate (BD Biosciences) were filled with 100 μl of each matrix. Matrices thickness was ~1 mm as measured by the number of rotations (subsequently converted in μm) of the fine focus knob of an inverted Microscope (ECLIPSE TS100 Nikon) from the surface of the matrix to the bottom membrane.

Extracellular matrix preparation. Fibrillar collagen I was prepared as described previously (22). Briefly, Nutragen (2 and 4 mg/ml final concentrations) was added to a mixture of 10% (v/v) MEM eagle 10× (MEM; Invitrogen, Carlsbad, CA), deionized water, and 4–6% (v/v) of 7.5% sodium bicarbonate buffer (pH 9) (Invitrogen). The preparation was loaded in Transwell inserts and allowed to polymerize for 30–40 min in an incubator at 37°C. Neutralization of the matrix was obtained by rehydratation of the matrix with 800 μl warm culture medium for at least 2 h in the incubator at 37°C 5% CO_2 before seeding the cells.

To obtain gelified fibrils from Nutragen collagen instead of a fibrillar network, we followed the manufacturer protocol. Briefly, 8 parts chilled Nutragen collagen were mixed with 1 part ice-cold 10× PBS (final concentration 5.1 mg/ml). The collagen preparation was then adjusted to pH 7.4 by addition of 67 μl 0.1 M NaOH and 33 μl 0.01 M HCl as monitored by pH paper. Then, the preparation was loaded in Transwell inserts, and gelation was started when incubated at 37°C for 1 h. Rehydratation was performed after the gelation by adding culture medium in the bottom chambers of Transwells 1 h before cell addition.

Matrigel was directly loaded in Transwell inserts, allowed to polymerize for 30 min, and rehydrated like fibrillar collagen.

To make the matrices easier to visualize by confocal microscopy, 0.25% (v/v) of 1 mg/ml FITC was added to the preparation of matrices where indicated. Matrices were then allowed to polymerize as described above and washed three times for 1 h at 37°C.

BD PuraMatrix was prepared as described by the manufacturer. After 30 min of polymerization, 400 μl culture medium was added on top of the matrix for 30–60 min, followed by three washes before cell addition.

Migration assay. After matrix polymerization, 1 ml of medium supplemented with 10% FCS (and 50 ng/ml M-CSF for MDMs) was placed in the lower chamber of the Transwell inserts to provide a chemoattractant gradient, and 280 μl of medium supplemented with 0.5% FCS was placed in the upper chamber on top of the matrices. Cells were starved for at least 4 h before the beginning of the experiment. Cells were harvested from the wells after a gentle wash in PBS, a 15-min treatment with PBS-EDTA (10 mM, pH 7.4), and centrifugation at 180 $\times$ *g* for 10 min at room temperature. Cells were resuspended in relevant medium without FCS, counted, and seeded on top of the matrices at 3–5 $\times$ 10^4 cells/Transwell inserts. Cells were then allowed to migrate for 2–3 d. The mixture of protease inhibitor (PI mix) was composed of E64c (100 μM), GM6001 (5 μM), aprotinin (0.04 TIU/ml), leupeptin (6 μM), and pepstatin (2 μM). Y27632 was used at 20 μM. DMSO at the concentration of PI mix was used as a control in all experiments. Inhibitor concentrations were established to obtain a good efficiency of the drugs without affecting cell viability as determined by trypan blue exclusion and lactate dehydrogenase release at the end of each experiment (68–72 h). The efficiency of protease inhibitors was determined by their ability to inhibit gelatin-FITC degradation by MDMs adhering on 2D surfaces (Supplemental Fig. 3). The efficiency of Y27632 was checked by the presence of the characteristic protrusive and highly branched cell phenotype on 2D surfaces and on top of all the matrices tested (data not shown). Inhibitors were added on top of the matrix 30 min before adding the cells and in the lower chamber at the same concentrations to allow for an optimal repartition of the inhibitors within the matrix. We also checked the diffusion of molecules in the different matrices using trypan blue solution placed either on top of the matrix or below in the lower chamber and noncolored medium in the other compartment, respectively. We observed that the equilibrium was reached after ~15 h in the different matrices.

Measurement of migration. Each 24 h, quantification of cell migration was performed using the motorized stage of an inverted video microscope (Leica DMIRB, Leica Microsystems, Deerfield, IL) and the Metamorph software. Pictures were taken automatically with a 10× objective and at constant 15-μm intervals, and cells on top and within the matrix were counted using the cell counter plugin of the ImageJ software (National Institutes of Health, Bethesda, MD). Percentage of migration was obtained as the ratio of the number of cells within the matrix to the total number of counted cells. Of note is that pictures were taken at the center and in the top two-thirds of the matrix and not on the sides or close to the membrane where the matrix stiffness might be different because of mechanical forces.

Phenotype quantification and calculation of aspect ratio. The phenotype of cells in the different 3D environment was quantified using the same pictures and Image J than for migration measurement. The aspect ratio is the ratio of the length of the major cell axis to the minor axis as described previously (31). For an amoeboid cell, the aspect ratio was <2.5, whereas for mesenchymal cells the aspect ratio was >2.5. For each condition, at least 100 cells were scored, and a minimum of three independent experiments were analyzed.

Scanning electron microscopy

Matrices were prepared and migration assay was performed as described above in the presence or absence of cells. Matrices were then fixed using 0.1 M sodium cacodylate buffer supplemented with 2.5% (v/v) glutaraldehyde and prepared as previously described (32) for observation with a JEOL JSM-6700F scanning electron microscope.

Live-cell imaging

Cells were embedded in matrices prior to polymerization of the lattice at least 16 h before starting of imaging. Imaging was performed using an inverted microscope (Leica DMIRB, Leica Microsystems) equipped with a motorized stage, an incubator chamber to maintain constant temperature, and CO_2 levels. Images were acquired with Metamorph software. In each experiment, 20× phase contrast time-lapse images were acquired every 10 min in 18–20 z-planes over a 5–12-h period for 7–10 representative fields of view per matrix. Cells were tracked in z-planes (15-μm step) in the central part of the gel away from the top and the bottom to avoid edge effects. A representative subset of time-lapse videos out of three independent experiments was analyzed using ImageJ software. To avoid problems of automated cell tracking, the manual motion tracking was used to track the center of the nuclei of each cell throughout the time sequence. Cell movement in the third dimension (z) was not considered for calculation of cell velocity, because it did rarely exceed five z-planes throughout the whole period of time. Quantification of cell migration velocity was calculated for each cell, and results are expressed as the mean ± SD of 15–26 cells coming from three independent experiments for each matrix. Cells were screened visually before selection, and nonmoving cells were not selected for analysis as described previously (31).

2D coatings

Coverslips were coated with 0.2 mg/ml FITC-coupled gelatin (Invitrogen) as described previously (32). For collagen I coating, 24-well coverslips were precoated with 2 μg/ml polylysine for at least 40 min at 37˚C. After a quick wash in PBS containing $CaCl_2$ and $MgCl_2$, BSA (0.5% final concentration) was added for 15 min at 37˚C. Thirty microliters of matrix was dropped off onto parafilm, and coverslips were returned onto it for a few minutes to obtain a thin layer adsorbed at the surface of polylysine coated coverslips. Coverslips were put back in empty wells for 40 min to allow collagen I polymerization at 37˚C. Coverslips were then washed in PBS, and cells ($3–5 \times 10^4$) were added.

Immunostaining, confocal microscopy, and image analysis

At the end of migration experiments, matrices were fixed with 3.7% (w/v) paraformaldehyde and 15 mM sucrose for 45min at room temperature. Paraformaldehyde was quenched with 50 mM NH_4Cl for 5min. Cells embedded in the matrices were permeabilized with PBS–Triton X-100 0.1% supplemented with 3% (w/v) BSA to perform saturation at the same time for 1 h. Then, cells were stained with primary Ab (5 μg/ml anti-paxillin, 80 μg/ml antigelsolin, 5 μg/ml anti–β_1-integrin, and 2 μg/ml anti–P-tyr) and secondary Ab, phalloidin-Texas Red (1 U/ml; Invitrogen), and DAPI (0.5 μg/ml; Sigma-Aldrich) or high-content screening (HCS) cell mask deep red (1 μg/ml; Molecular Probes, Eugene, OR). For cortactin labeling, a 7-min prefixation step was performed in PFA 3.7% and 0.3% Triton X-100, and no further permeabilization was done before the addition of the primary Ab (10 μg/ml anticortactin). The protocol was then followed as for the other Abs.

Type I collagen degradation can be assessed by detecting the C-terminal neoepitope generated by collagenase-mediated cleavage of collagen triple helix (the 3/4 fragment). This neoepitope was visualized using the anti-COL2 3/4 C_{short} IgG (IBEX Pharmaceuticals) as described previously (22).

Images were collected using a confocal microscope (Leica SP2). Samples were scanned with a 0.1–0.4-μm step. Images were processed for brightness and contrast and filtered for noise with Adobe Photoshop according to the current ethical lines (33).

Rheology of reconstituted matrices

Matrix responses to oscillatory shear was measured using a rheometer (Advanced Rheometer AR1000) equipped with a cone (diameter: 40 mm; angle: 2˚)/flat-plate geometry. This standard geometry consists of a horizontal plate (flat-plate) topped with a cone, the sample being sandwiched between the lower plate and the upper cone. The plate was first refrigerated at 10˚C. A matrix sample in liquid form (600 μl), prepared as above at 4˚C, was placed on the center of the lower plate. The cone was lowered onto the sample to the proper height. The plate was heated to 37˚C, and the samples were left undisturbed for 30 min to allow for gel formation. A humid atmosphere was created around the plates. After 30 min, the sample was subjected to oscillatory shear by rotating the cone around its axis with a maximum strain of 1%, with an angular velocity that oscillates sinusoidally. Both storage modulus (G') and loss modulus (G") were measured in the linear viscoelastic regimen as a function of the frequency of the angular velocity from 0.1–1 Hz.

Statistical analysis

Data are reported as mean ± SD. Statistical comparisons between three or more sets of data were performed with a bilateral Student paired *t* test. Values of $p < 0.05$ are represented by one star, < 0.01 by two stars, and < 0.001 by three stars.

Online supplemental material

Results obtained with HT1080 cells are shown in Supplemental Fig. 1. Quicktime movies of the image series from which Figs. 1–4 were made (Supplemental Videos 1–4) and original scanning electron microscopy pictures (Supplemental Fig. 2) are available. Results obtained on the effect of protease inhibitors on podosomes and FITC-gelatin degradation are shown in Supplemental Fig 3.

Results

To unravel human MDM 3D migration, we chose the 3D migration models currently used in studies with invasive tumor cells, which are acellular ECM composed of either fibrous collagen I or Matrigel (9, 12, 34). We developed an experimental model in which ECM is thick enough to observe a 3D phenotype and measure parameters of 3D migration.

Human macrophages exhibit a mesenchymal migration mode in Matrigel with no mesenchymal-to-amoeboid transition

First, we studied human MDM 3D migration through thick layer of Matrigel. This matrix is a mixture of ECM proteins produced by a mouse sarcoma cell line grown in vivo, particularly rich in laminin and collagen IV, and is structurally organized as a gel (35). At the surface of the matrix, MDMs were round or spindle shaped but almost exclusively elongated inside the matrix (Fig. 1*A–C*, Table I), as observed by: 1) phase-contrast microscopy pictures of living cells (Fig. 1*A*); 2) confocal fluorescence microscopy and z-reconstitutions of fixed cells (Fig, 1*B*, *left panel*); and 3) by scanning electron microscopy (Fig. 1*C*).

We then examined MDM migration in the presence of a mixture of proteases inhibitors (PI mix) previously used by other groups to characterize the migration mode of tumor cells (15, 18). It contains the broad MMP inhibitor GM6001, the non-membrane-permeable thiol proteases inhibitor E64c, the serine protease inhibitor aprotinin, the broad cysteine protease inhibitor leupeptin, and the aspartic protease inhibitor pepstatin. When PI mix was added, macrophage infiltration into the matrix was strongly affected (Fig. 1*D*), and the presence of holes in the matrix observed by scanning electron microscopy around MDMs, which penetrated into Matrigel (Fig. 1*C*, arrows), was much less frequently detected. When GM6001 was used alone at 10 μM (Fig. 1*D*) or at the concentration of PI mix (5 μM; data not shown), no inhibition of macrophage migration was observed. To confirm that MMPs are not involved in the protease-dependent migration of human macrophages, the peptidomimetic inhibitors of MMPs, BB-94/Batimastat (5 μM) or BB-2516/Marimastat (1.5 μM) (16, 36), were used, and no inhibition was observed (data not shown). When the molecules present in PI mix, except GM6001 were used together, macrophage migration was inhibited but not as efficiently as PI mix (Fig. 1*D*).

The dependence on matrix remodeling was also illustrated by the use of the proteolysis-resistant dense matrix, BD PuraMatrix Peptide Hydrogel, which like Matrigel, polymerizes into a 3D dense hydrogel (37). Even after 7 d on PuraMatrix used at comparable concentration than Matrigel (10 mg/ml) or twice diluted, human MDMs were unable to pierce into this matrix (data not shown).

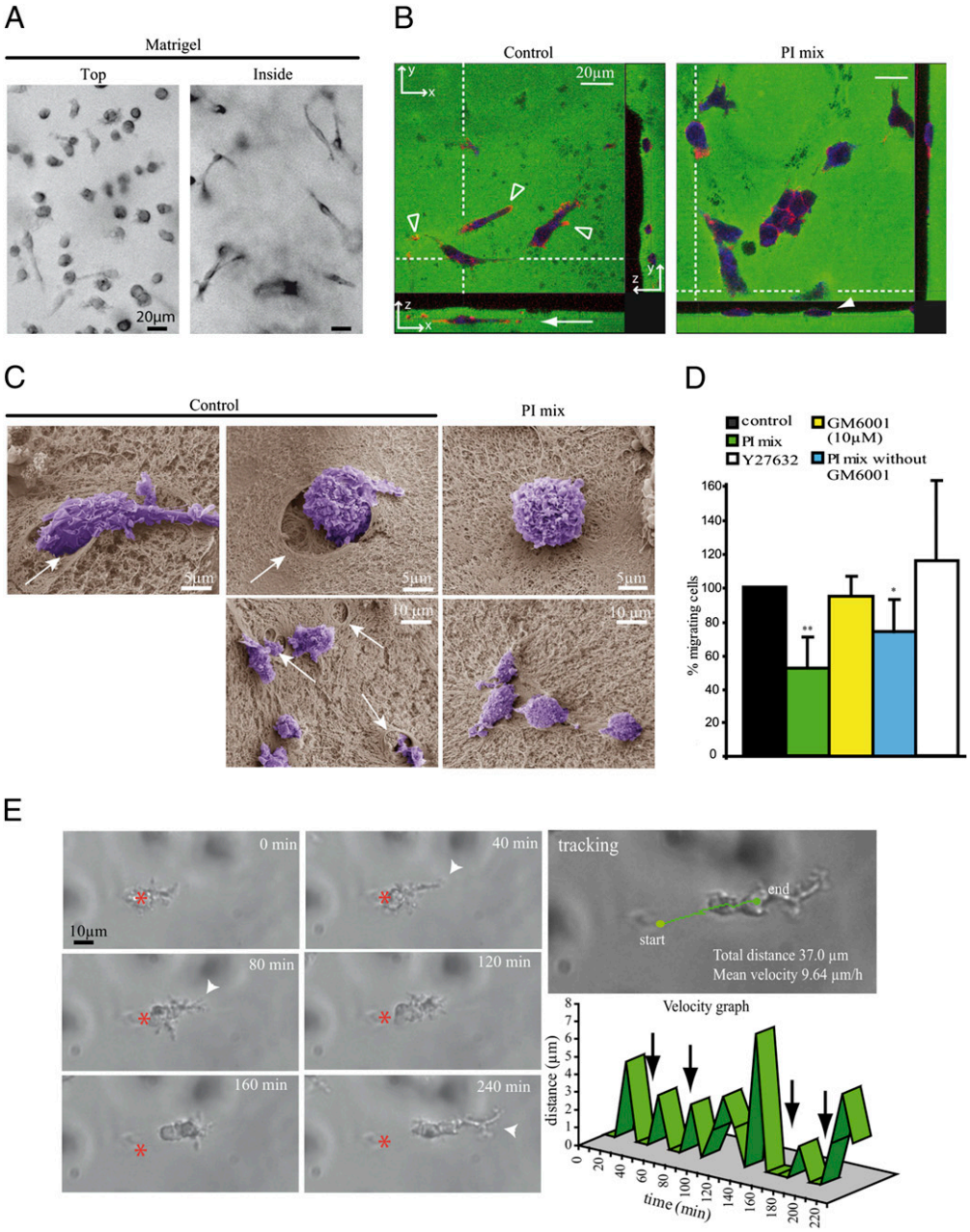

FIGURE 1. Human macrophages use the mesenchymal mode to migrate through Matrigel in a protease-dependent but MMP-dispensable manner. Human MDMs were loaded on the top of thick layers of Matrigel (9.3–11 mg/ml) polymerized in Transwell inserts. Cell migration was monitored every 24 h, and pictures of cells were taken after 72 h (*A–C*). *A*, Pictures of live cells either at the surface (top) or within (inside) the matrix were taken using the inverted video microscope (original magnification ×40). Bars: 20 μm. *B*, Confocal images of cells migrating in FITC-labeled matrices in the presence (PI mix) or absence (control) of protease inhibitors. Cells were fixed and permeabilized prior to staining of F-actin with Texas Red phalloidin and cell body with HCS cell mask deep red. Projections of a single z-section and x/z and y/z projections along the dashed white lines are shown. Elongated cells were observed within the matrix (arrow). Cells on the top of Matrigel showed mostly a rounded shape (white arrowheads). F-actin–enriched structures at the tip of membrane protrusions are shown (open arrowheads) using the Leica SP2 confocal microscope (original magnification ×40). Bars: 20 μm. *C*, Morphology of cells and interaction with the surrounding matrix was analyzed by scanning electron microscopy. Note the presence of holes in the matrix around control cells penetrating Matrigel (arrows), which were only occasionally seen in PI-treated cells (*right pictures*) (top, original magnification ×3000; bottom, original magnification ×1200). Bars: 5 and 10 μm. *D*, The percentage of migrating cells was measured in control or drug-treated cells (PI mix, GM6001 at 10 μM, PI mix without GM6001 or Y27632). Results are expressed as normalized values (mean ± SD of at least three independent experiments). Percentage of migrating cells in control experiments 26.7 ± 11.1%, $n = 7$. Statistics: Student t test ($p = 0.005$ for PI mix). *E*, Human MDMs were embedded in Matrigel for 24–48 h, and cell movement was followed by time-lapse video microscopy using the Leica DMIRB inverted microscope equipped with a CoolSnap HG camera (Roper Scientific SAS, Evry, France) (original magnification ×20). (Movie is shown in Supplemental Video 1). Initial position of the nucleus is labeled with a red asterisk. Arrowheads show protrusions at the leading edge and bifurcation between two branched pseudopodia typical of mesenchymal migration. Cell migration was discontinuous with short stops between two nucleus movements (arrows in the velocity graph) but directional as shown by the straightforward trajectory of cell (tracking). All experiments were repeated at least three times. Bar: 10 μm.

Table I. *Percentage of protrusive MDMs within the different matrices in the presence (PI mix) or in the absence (control) of protease inhibitors*

% Protrusive Cells	Matrigel	Fibrillar Collagen I	Gelled Collagen I
Control	84 ± 1.4	23 ± 6	67 ± 13
PI mix	63 ± 6.5*	20 ± 16	57 ± 25

MDMs were allowed to migrate for 48–72 h. The aspect ratio of at least 100 cells was calculated. Cells were determined as protrusive when the ratio was >2.5. The percentage of protrusive cells in gelled collagen I and Matrigel were high compared with fibrillar collagen I. In both Matrigel and gelled collagen I, PI mix induces a small decrease of protrusive cells compared to control; the difference is statistically significant in Matrigel (*). Values are mean ± SD of at least three independent experiments.

In contrast to PI mix, when the ROCK inhibitor Y27632 was used in the Matrigel migration assay, MDM migration capacity was not affected (Fig. 1*D*).

MDM migration observed by live imaging showed a typical mesenchymal movement with long and branched leading pseudopodia (Fig. 1*E*, arrowheads) and a back tail that retracted (Supplemental Video 1). Cell movement was slow (11.7 ± 2.9 μm/h; Fig. 2*A*, *left panel*) compared with migration of tumor cells (20), directional as shown by cell tracking (Figs. 1*E*, 2*A*, *left panel*) and saltatory as illustrated in Fig. 1*E* (velocity graph, black arrows) with cell nuclei staying immobile for a long period of time and then moving suddenly before becoming static again. Interestingly, a second type of cell movement that we called "fast" movement was also observed in this matrix, which is bidirectional and the fastest (29.0 ± 9.8 μm/h; Fig. 2*A*, *right panel*, 2*B*). This movement proceeded along a tunnel that persisted into the matrix with alternate back and forth movements (Fig. 2*B*, Supplemental Video 2) as described for endothelial cells (38) and tumor cells (39).

Taken together, these results indicate that: 1) human MDMs migrate through Matrigel via the mesenchymal mode and thus show that leukocyte migration is not restricted to a protease-independent mode; and 2) the protease-dependent migration mode of human MDMs is not inhibited by MMP inhibitors, in contrast to tumor cells. As the amoeboid migration mode of U937 macrophages has been previously described in fibrillar collagen I matrix (22), we next used this matrix to study MDM 3D migration.

Human macrophages exhibit an amoeboid migration mode in fibrillar collagen I

Collagen I is the most abundant collagen in human body. Fibrillar collagen I is used to mimic classical stromal/interstitial ECM. Matrigel and fibrillar collagen I matrices had very different structures as shown by scanning electron microscopy pictures (Figs. 1*C*, 3*C*, respectively). Matrigel formed a dense material, whereas collagen I formed a highly porous matrix, in which long fibers can be clearly identified (12). Both at the surface and within fibrillar collagen I, most MDMs exhibited a rounded shape as shown in Fig. 3*A*, Fig. 3*B*, *left panel*, and Fig. 3*C*, *left picture*, and few cells had a protrusive phenotype (Table I).

When Y27632 was added to the migration assay, cell migration was strongly inhibited (Fig. 3*D*), showing that MDM migration was dependent on ROCK activity. When protease inhibitors were added, the phenotype of the cells (Fig. 3*B*, 3*C*, Table I), and the percentage of migrating MDMs were unchanged compared with untreated cells (Fig. 3*D*).

By time-lapse video microscopy, we observed that MDMs performed a typical amoeboid movement with rounded membrane protrusions (40, 41) and few short protrusions (Fig. 3*E*, Supplemental Video 3). Cell movement was much less saltatory than in Matrigel (Fig. 3*E*, velocity graph) and not directional as shown by cell tracking (Fig. 3*E*, *right picture*, 3*F*). The mean velocity was of 42.5 ± 17.2 μm/h (Fig. 3*F*), which was 3.6 times faster than in Matrigel.

These results demonstrate that human MDMs adopt an amoeboid migration mode in fibrillar collagen I.

In contrast to MDMs, in fibrillar collagen I, HT1080 tumor cells have a mesenchymal migration mode (18, 20). We actually observed

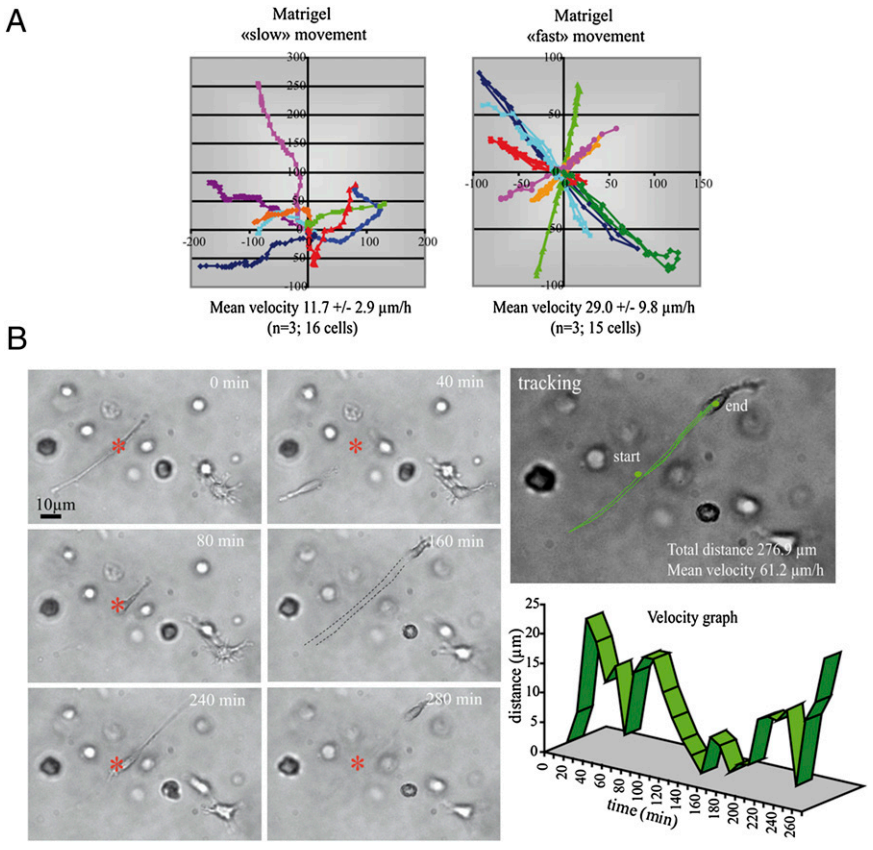

FIGURE 2. *A*, Tracking of human MDMs migrating through Matrigel. Human MDM trajectories were analyzed. Cells (number indicated) were examined by time-lapse video microscopy. The mean velocity was calculated, and the x/y trajectory of seven representative cells is shown on the graphs with a different color for each cell. Starting point is at the origin and each following point represents the position of the cell at 10-min time interval. Two types of cell movement were monitored: a "slow" movement, which was unidirectional, and a "fast" movement with alternate forward and backward motions. The latter proceeded along a tunnel that persisted into the matrix. *B*, Time-lapse video microscopy imaging of the "fast" movement of MDMs in Matrigel, which was taken using the Leica DMIRB inverted microscope equipped with a CoolSnap HG camera (original magnification ×20). (Movie is shown in Supplemental Video 2.) MDMs were treated as described in Fig. 1*E*. Initial position of the nucleus is labeled with a red asterisk. The persistent tunnel is materialized by dashed black lines at time point 160 min. All experiments were repeated at least three times. Bar: 10 μm.

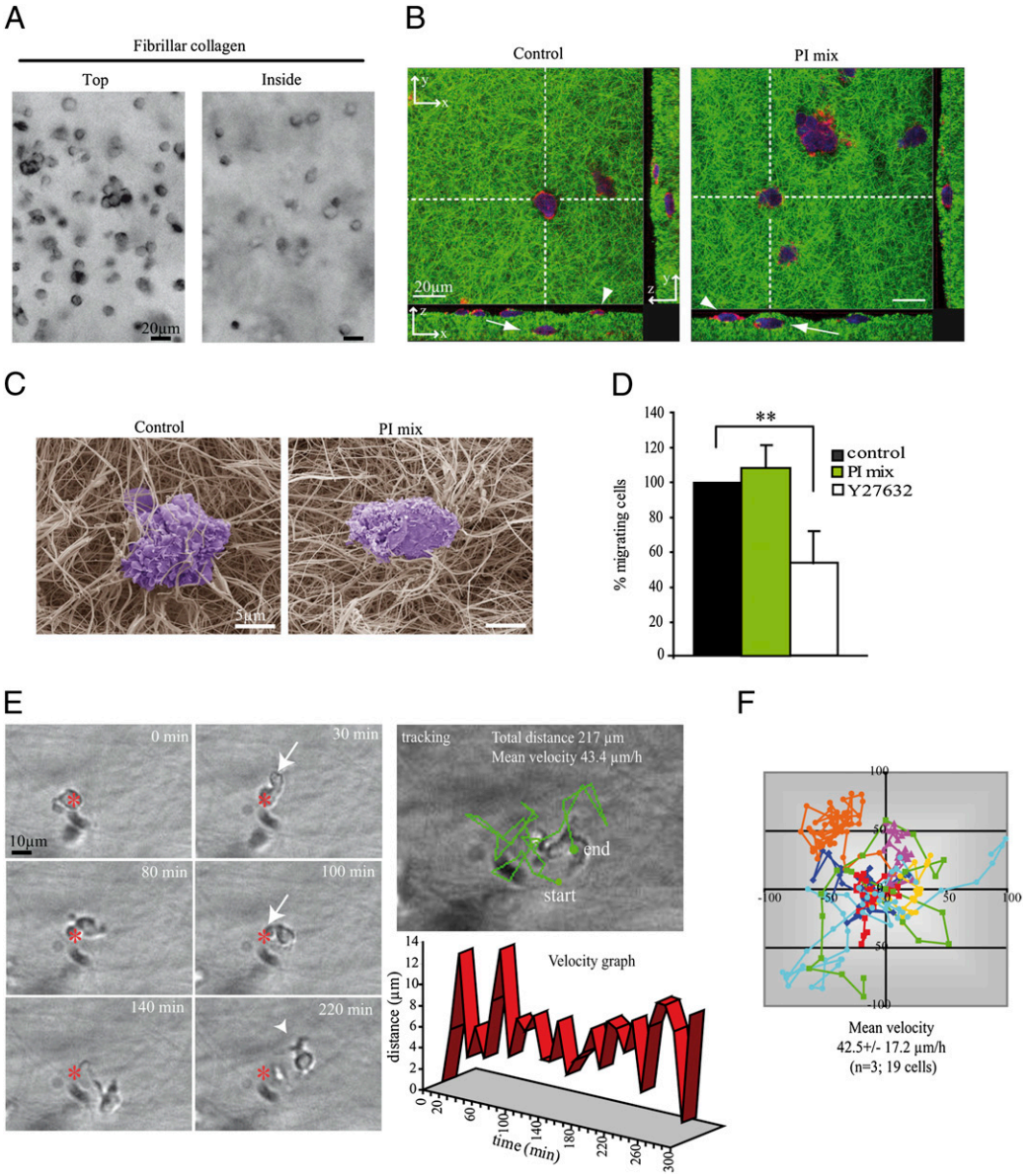

FIGURE 3. Human macrophages use the amoeboid mode to migrate through fibrillar collagen I. Human MDMs were loaded on the top of thick layers of fibrillar collagen I (2 mg/ml) polymerized in Transwell inserts. Cell migration was monitored every 24 h, and pictures were taken after 48 h (*A–C*). *A*, Pictures of live cells either at the surface (top) or within (inside) the matrix were taken using an inverted video microscope (original magnification ×10). Bars: 20 µm. *B*, Confocal pictures as described in Fig. 1 are showing cells migrating through FITC-labeled collagen in the presence (PI mix) or absence (control) of protease inhibitors. They were fixed and permeabilized prior to staining of F-actin with Texas Red phalloidin and cell body with HCS cell mask deep red. Control and PI mix-treated cells behaved similarly: equivalent proportion of cells at the surface (arrowheads) or within (white arrows) the matrix and similar morphology and F-actin staining in both cases (Leica SP2 confocal microscope, original magnification ×40). Bars: 20 µm. *C*, Scanning electron microscopy pictures of control and PI mix-treated cells on the top of fibrillar collagen were taken (original magnification ×3500). Bars: 5 µm. *D*, The percentage of migrating cells was measured in control or drug-treated cells (PI mix or Y27632). Results are expressed as normalized values (mean ± SD of at least three independent experiments), the percentage of migrating control cells is 33.8 ± 8.9% ($n = 7$). Statistics: Student t test ($p = 0.007$ for Y27632). *E*, Human MDMs were embedded in fibrillar collagen, and cell movement was followed by time-lapse video microscopy for indicated times using the Leica DMIRB inverted microscope equipped with a CoolSnap HG camera (original magnification ×20). (Movie is shown in Supplemental Video 3.) Initial position of the nucleus is labeled with a red asterisk. Rounded membrane protrusions (arrows) and few short protrusions (arrowheads) characteristic of amoeboid migration are shown. Cell movement was continuous (velocity graph) but not directional as shown by the random trajectory of cell (tracking). All experiments were repeated at least three times. Bars: 10 µm. *F*, Trajectories of 19 human MDM in three independent experiments were followed by time-lapse video microscopy. The mean velocity was calculated, and the x/y movement of seven representative cells is shown on the graphs with a different color for each cell trajectory. Starting point is at the origin, and each following point represents the position of the cell at each 10-min time interval. Compare the random continuous movement in fibrillar collagen to the orientated discontinuous movement in Matrigel (Fig. 2).

that they exhibited a mesenchymal morphology (Supplemental Fig. 1*A*). In the presence of protease inhibitors, the characteristic mesenchymal-amoeboid transition was observed with a decreased percentage of protrusive HT1080 cells and a constant migration rate (Supplemental Fig. 1*A*) as described previously (20).

To conclude on these first two parts, we showed that human MDMs are able to perform either amoeboid or mesenchymal migration depending on the matrix. In contrast to tumor cells, mesenchymal migration in Matrigel is not affected by MMP inhibition.

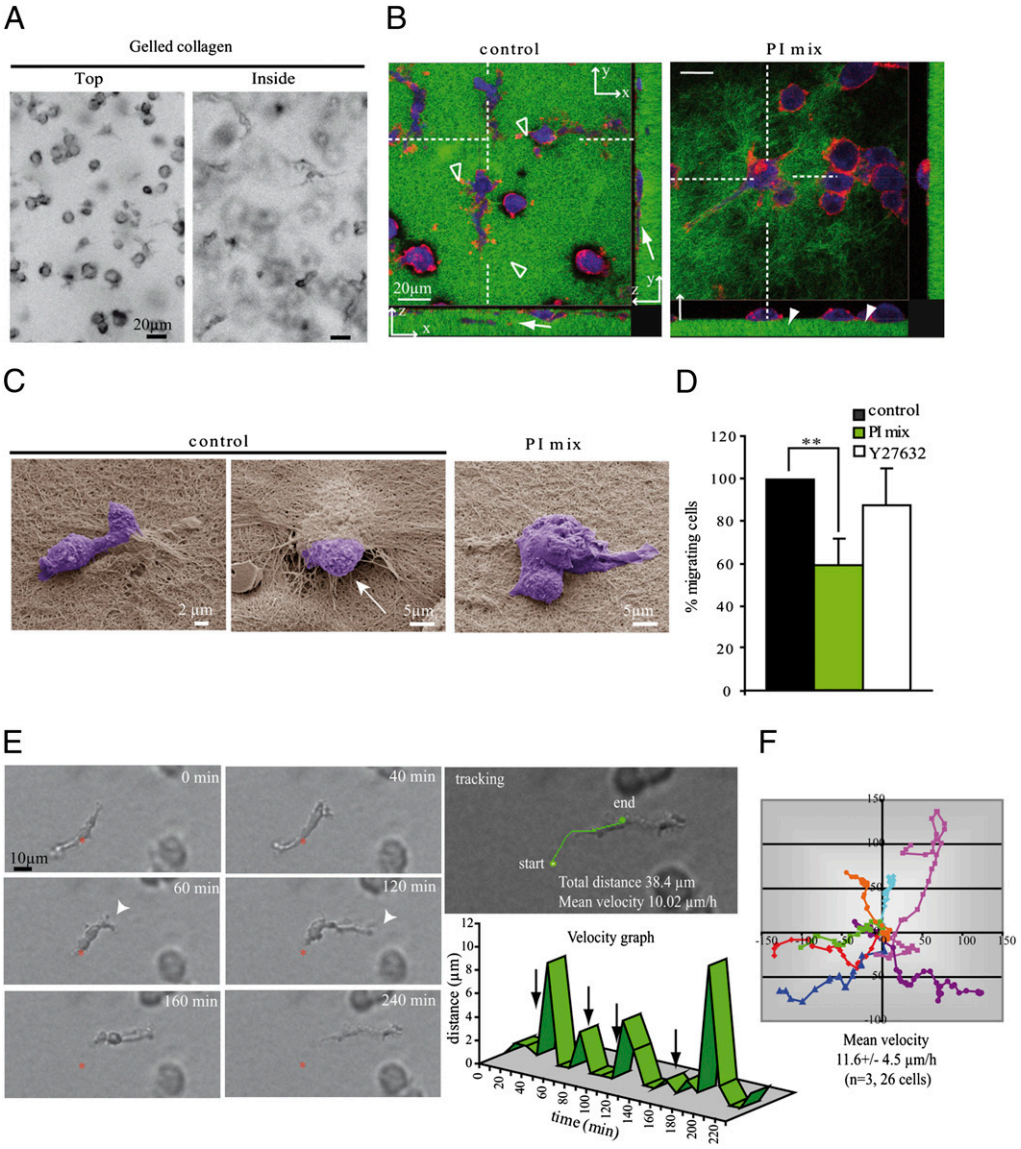

FIGURE 4. Human macrophages use the mesenchymal mode to migrate through a matrix of collagen I structurally organized as a gel. Human MDMs were loaded on the top of thick layers of gelled collagen I (5.1 mg/ml) polymerized in Transwell inserts. Cell migration was monitored every 24 h, and pictures of cells were taken after 72 h (*A–C*). *A*, Pictures of live cells either at the surface (top) or within (inside) the matrix were taken using an inverted video microscope (original magnification ×10). Bars: 20 μm. *B*, Confocal images as described in Fig. 1 are showing cells migrating in FITC-labeled matrices in the presence (PI mix) or absence (control) of protease inhibitors. Cells were fixed and permeabilized prior to staining of F-actin with Texas Red phalloidin and cell body with HCS cell mask deep red. Elongated cells were observed within the matrix (arrow). Cells on the top of collagen showed mostly a rounded shape (white arrowheads). F-actin enriched structures at the tip of membrane protrusions are shown (open arrowheads) (Leica SP2 microscope, original magnification ×40). Bars: 20 μm. *C*, Morphology of cells and interaction with the surrounding matrix analyzed by scanning electron microscopy (original magnification ×3500). Dismantled matrix is observed at the place of penetration of control cell inside collagen (arrow). This was not observed in the presence of PI mix. Bars: 2 and 5 μm. *D*, The percentage of migrating cells was measured in control or drug-treated cells (PI mix or Y27632). Results are expressed as normalized values (mean ± SD of at least three independent experiments), the percentage of migrating control cells is 33.0 ± 9.1% ($n = 5$). Statistics: Student t test ($p = 0.002$ for PI mix). *E*, Human MDMs were embedded in gelled collagen I, and cell movement was followed by time-lapse video microscopy using a Leica DMIRB inverted microscope equipped with a CoolSnap HG camera (original magnification ×20). Initial position of the nucleus is labeled with a red asterisk. Like in Matrigel, cells showed protrusions at the leading edge and bifurcation between two branched pseudopodia (arrowheads), cell migration was discontinuous with short stops between two nucleus movements (arrows in the velocity graph), and cell trajectory was directional (straightforward movement of cell on the tracking picture). (Movie is shown in Supplemental Video 4.) Each experiment was repeated at least three times. Bars: 10 μm. *F*, Trajectories of 26 human MDMs in three independent experiments were followed by time-lapse video microscopy as described in Fig. 3*F*, trajectories of seven representative cells are shown on the graphs with a different color for each cell. Compare the orientated discontinuous movement to the random continuous movement in fibrillar collagen (Fig. 3).

Human macrophages exhibit a mesenchymal migration mode in collagen I matrix when structured as a gel

Because fibrillar collagen I and Matrigel have distinct biochemical compositions, we made up a new matrix by using the same collagen I polymerized as a dense gel, which we called gelled collagen I.

When human MDMs were loaded on gelled collagen I, cell migration characteristics were identical to those observed with Matrigel: a majority of rounded cells at the surface and protrusive cells within the matrix (Fig. 4*A*, 4*B*), and *trans*-matrix migration was dependent on protease activity as shown by the inhibitory

effect of PI mix on cell migration (Fig. 4*B–D*). Like in Matrigel (Fig. 1*D*), GM6001 used alone did not impair macrophage migration in gelled collagen I (data not shown). The percentage of protrusive cells was not significantly decreased in the presence of PI mix (Fig. 4*C*, Table I), and instead of the well-delimited holes observed in Matrigel (Fig. 1*C*), gelled collagen I appeared dismantled at the place of cell penetration (Fig. 4*C*, arrow).

In addition, no significant inhibition of cell migration was observed in the presence of the ROCK inhibitor Y27632 (Fig. 4*D*) and cell migration showed a typical mesenchymal movement (Fig. 4*E*, Supplemental Video 4) with long leading pseudopodia (Fig. 4*E*, arrowheads), oriented (Fig. 4*E* ,tracking, 4*F*) and saltatory cell movements (Fig. 4*E*, velocity graph arrows). The mean velocity was 11.6 ± 4.5μm/h (Fig. 4*F*), which was very close to the "slow" movement observed in Matrigel. These results are in favor of migration of MDMs within gelled collagen through the mesenchymal mode.

So, although both matrices were made of collagen I, human MDMs were able to develop two distinct modes of 3D migration, amoeboid and mesenchymal, depending on whether it is organized as fibers or gel. This suggested that MDM migration mode could be influenced either by the architecture (gel or fibers) or by the rigidity of the matrix.

For comparison, HT1080 cells adopted a similar mesenchymal morphology in gelled collagen than in fibrillar collagen (Supplemental Fig. 1). However, in the presence of PI mix, the percentage of protrusive cells was decreased and HT1080 cells migration was broadly inhibited (Supplemental Fig. 1*B*), suggesting that the mesenchymal/amoeboid transition cannot occur in this matrix like it does in fibrillar collagen. Thus, the behavior of HT1080 cells in gelled collagen I mimics the one described in native fibrillar collagen I (Supplemental Fig. 1) (16).

The choice of macrophage migratory mode is dictated by the ECM architecture

Next, we examined the influence of parameters existing in 3D environments, such as porosity and elasticity of the matrix.

Regarding the architecture of matrices, scanning electron microscopy pictures provided information about the structural organization of the matrices used in this study (Fig. 5*A*). Like Matrigel, gelled

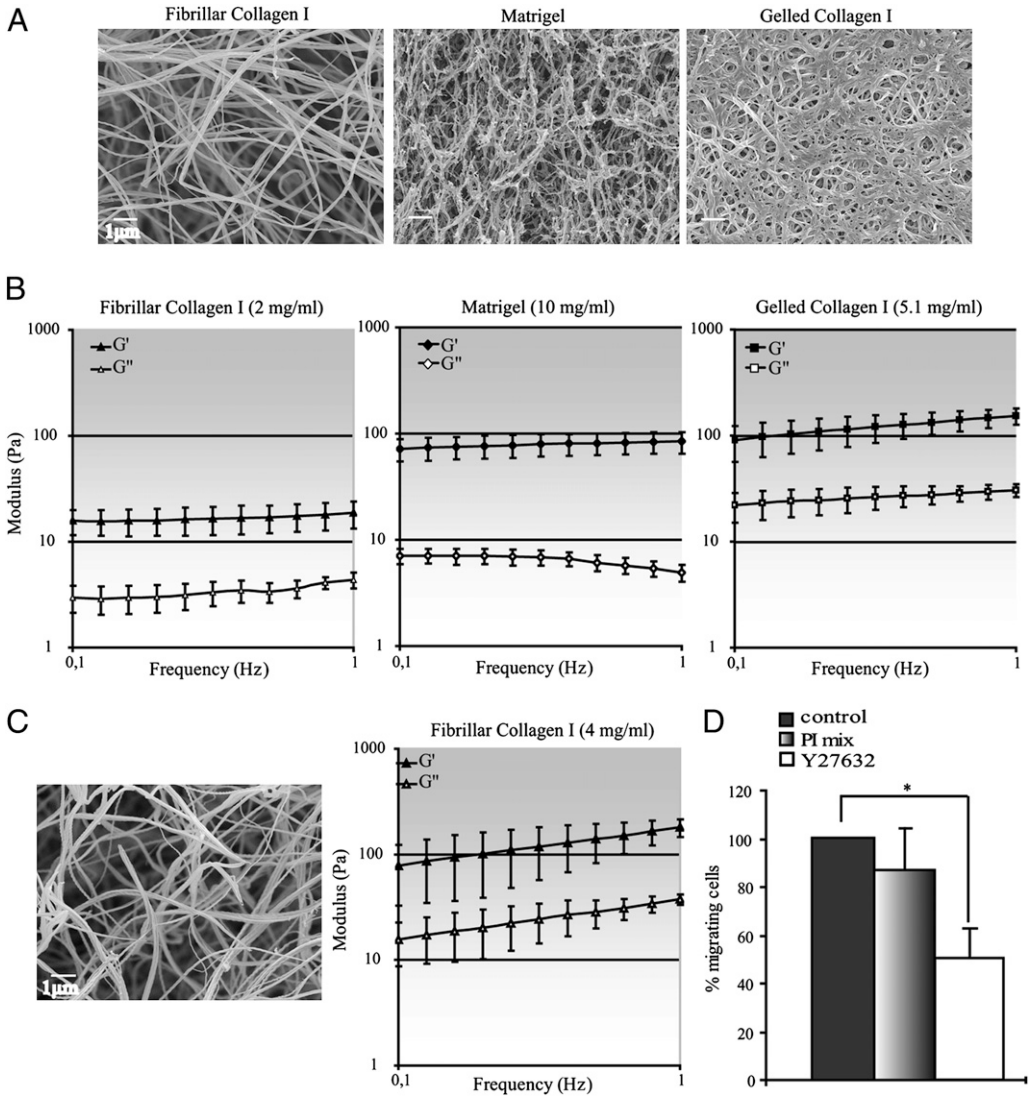

FIGURE 5. Physical parameters of matrices. *A*, Distinct structural organizations of matrices is shown by pictures of fibrillar collagen I (2 mg/ml), Matrigel (10 mg/ml), and gelled collagen I (5.1 mg/ml) examined by scanning electron microscopy (original magnification ×10,000). Bars: 1 μm. *B*, Matrix rigidity values are shown by rheometry measurement of G' and G" moduli of each matrix. *C* and *D*, Fibrillar collagen I at 4 mg/ml was used. *C*, Scanning electron microscopy picture and rheometry measurement of G' and G" moduli; bar: 1 μm (original magnification ×10,000). *D*, Percentage of migrating cells in control or drug-treated cells (PI mix or Y27632) after 48 h. Results are expressed as mean ± SD of three independent experiments, and the percentage of migrating control cells is of 37.5 ± 10.1% ($n = 4$). Statistics: Student t test ($p = 0.022$ for Y27632).

collagen I was a dense network of small interfiber spaces, whereas fibrillar collagen I was made of long fibrils with large interfiber spaces.

Rheological measurements were undertaken to provide information about the mechanical characteristics (elasticity and viscosity) of the matrices. The matrices were subjected to a small-amplitude oscillatory shearing. For each matrix tested, the elastic modulus (G') and the viscous modulus (G") were recorded in function of the frequency (Fig. 5*B*). Both moduli remained almost unchanged through the frequency range, with G' always greater than G". This behavior is typical of a solid-like material. More precisely, when G' is one order of magnitude higher than G" it relates to a "weak gel" material (42, 43). As shown in Fig. 5*B*, gelled collagen I and Matrigel had comparable elasticity but Matrigel had a lower viscosity. In comparison, these two parameters were much lower in fibrillar collagen.

To explore whether the different migration modes could be controlled by differences in matrix visco-elastic properties rather than architectural properties, we next prepared a matrix of fibrillar collagen with visco-elastic properties similar to that of gelled collagen at 5.1 mg/ml. We found that this (Fig. 5*B*) was reached by increasing the concentration of fibrillar collagen at 4 mg/ml (Fig. 5*C*). Under these conditions, MDMs seemed to perform amoeboid migration as defined by the characteristic rounded phenotype (data not shown), with a significant inhibitory effect of Y27632 but no significant effect of PI mix (Fig. 5*D*).

These results indicate that, in collagen I matrices with similar visco-elastic properties but distinct architectures (very large versus small pores), human MDMs are able to perform either amoeboid or mesenchymal migration mode. It is likely that MDMs adapt their migration mode to the geometry of the matrix.

Human MDMs performing mesenchymal migration exhibit collagenolytic protrusions

We next wanted to better characterize human MDM mesenchymal migration.

Macrophages are equipped with specialized structures called podosomes with ECM proteolytic properties (44, 45) like their tumoral counterpart, invadopodia (46). So, we examined whether these structures, which have only been studied in two dimensions (47), could be involved in the 3D protease-dependent migration mode of macrophages.

As the formation of invadopodia has been shown to be strongly inhibited in the presence of MMP inhibitors (48), we first examined this possibility in human macrophages. As shown in Supplemental Fig. 3, the proteolytic activity of podosomes but not their formation was strongly affected in the presence of PI mix or GM6001. Next, we examined whether the classical macrophage podosomal structures were formed in MDMs adhering on gelled and fibrillar collagen I polymerized on glass coverslips as thin layers to maintain the cells in two dimensions. When compared with the cell shape in Figs. 3 and 4, MDMs layered on the two 2D matrices were flat (Fig. 6*A*) as expected from previous data showing that cells flattened as the stiffness of the matrix increased (42, 49, 50). In addition, they formed podosomes characterized by the classical F-actin dots and matrix degradation was observed (Fig. 6*A*, arrows).

Finally, human MDMs migrating in three dimensions within a thick layer of the same matrices were fixed and proteins commonly observed in podosomes or invadopodia (47, 51–53) were stained. Inside gelled collagen, the tips of membrane protrusions formed by MDMs were enriched in F-actin (Figs. 4*B*, 6*B*), cortactin, paxillin, gelsolin, and P-tyr proteins (Fig. 6*B*). Integrins are cell adhesion receptors, which mediate leukocyte migration (54). β_1-integrin is the main collagen I receptor (3); it is associated to invadopodia and podosomes (34, 52) and involved in tumor cell invasion (55). In this study, we found β_1-integrin colocalizing with F-actin at the tips of pseudopodia (Fig. 6*B*). At the interface between F-actin–rich protrusions and the matrix, collagenolysis was observed using Abs specifically recognizing cleavage-site–specific epitopes of collagen I, COL2 3/4 C short Abs (Fig. 6*B*) as previously reported for tumor cells (56). When MDMs migrated inside fibrillar collagen, these F-actin–rich protrusions were not observed. Cortactin, paxillin, gelsolin, β_1-integrin, and tyrosine-phoshorylated protein stainings were diffuse and collagenolysis epitopes were not detected (Fig. 7).

These results suggest that collagenolytic protrusions are only formed when the migration mode requires defined proteolytic activity and thus could be the 3D organization of podosomes.

Discussion

A hallmark of leukocytes is their ability to migrate through anatomical barriers. They share this property with invasive tumor cells. Although 2D migration of leukocytes is well described, 3D migration, which takes into account the interstitial tissue physical constraints, has been documented mostly for T lymphocytes and dendritic cells but not for macrophages (3, 57). We report in this study that human MDMs are able to perform either amoeboid or mesenchymal migration. They are the first cells able to adapt their migration mode to the matrix architecture. Finally, we show that macrophage mesenchymal migration involves proteolytic activity located at the tip of membrane protrusions, which could be the 3D counterparts of 2D podosomes.

In the course of in vivo migration, macrophages encounter interstitial tissues structured as collagen I fibers or as gel in basement membranes and dense tissues, such as tumors (3, 7, 58). So, our first attempt has been to examine the migration of human MDMs in matrices presenting these two different network structures, i.e., fibrillar collagen I and Matrigel, both being commonly used to study tumor cell migration. Furthermore, we designed a new matrix that we called gelled collagen I, which shares the biochemical composition with fibrillar collagen I and the architecture with Matrigel. Most of the experiments were designed to compare in parallel the migration modes of MDMs from the same donor in the three matrices used in this article. We observed that MDMs from all of the donors used in this study (>15) are able to adapt their migration mode to the matrix, performing either amoeboid movement in fibrillar or mesenchymal migration in gelled matrices. But, in contrast to tumor cells, human macrophages are unable to overcome the action of protease inhibitors by mesenchymal-amoeboid transition. The use of pepsin-extracted collagen I polymerized as fibrils has been shown to be permissive for amoeboid migration of tumor cells while native fibrillar collagen I, with similar pore size but distinct collagen I intermolecular cross-links, triggers protease-dependent migration (16). As we used pepsin-extracted collagen I, it will be interesting to investigate whether macrophages migrating in fibrillar native collagen I perform the mesenchymal migration mode. Nevertheless, an important finding of the present work is that human MDMs perform protease-dependent 3D migration depending on the matrix architecture and not only amoeboid movements as previously assumed.

In light of these results, our next attempt was to understand which parameter of the matrix motivates MDMs to do mesenchymal or amoeboid migration: the viscoelastic properties or the architecture of the matrix. To study the consequences of the matrix structure onto the macrophage migration mode, matrices with the same biochemical composition (collagen I) and the same viscoelastic properties were used. In fibrillar collagen, macrophages perform amoeboid migration, and in gelled collagen, they use mesenchymal migration, suggesting that macrophages are able

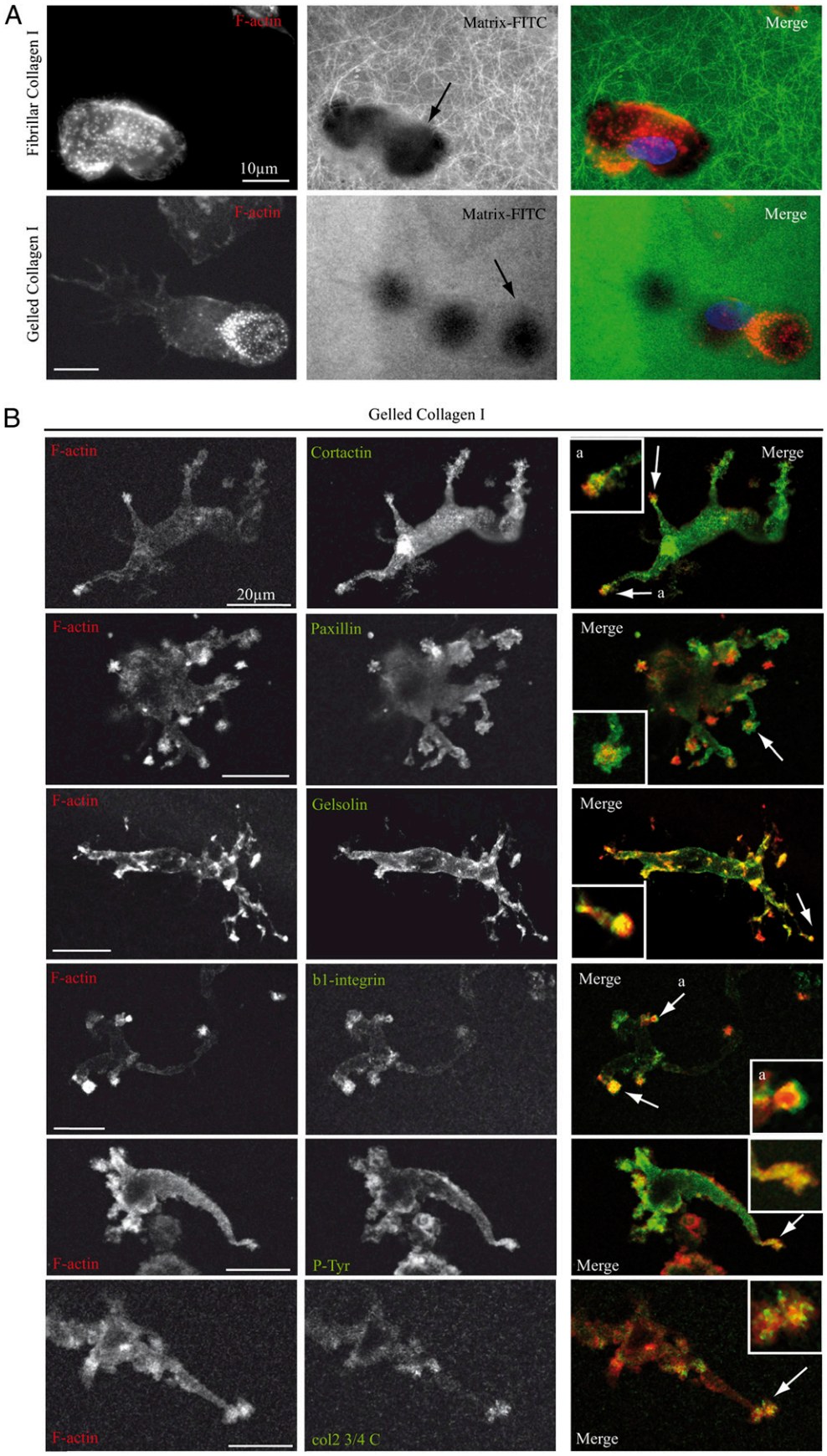

FIGURE 6. *A*, Human MDMs adherent on 2D fibrillar and gelled collagen form podosomes and degrade the matrix. Cells were loaded on glass coverslips coated with a thin layer of FITC-labeled fibrillar or gelled collagen I. After 16 h of adhesion, cells were fixed and stained for F-actin with Texas Red phalloidin. Note that cells are flattened, form podosomes (F-actin–enriched dots), and degrade the matrix underneath the cells on the two matrices (arrows). The holes in the FITC matrix were frequently below F-actin–rich podosomes. Holes that did not coincide with F-actin could correspond to podosomes that

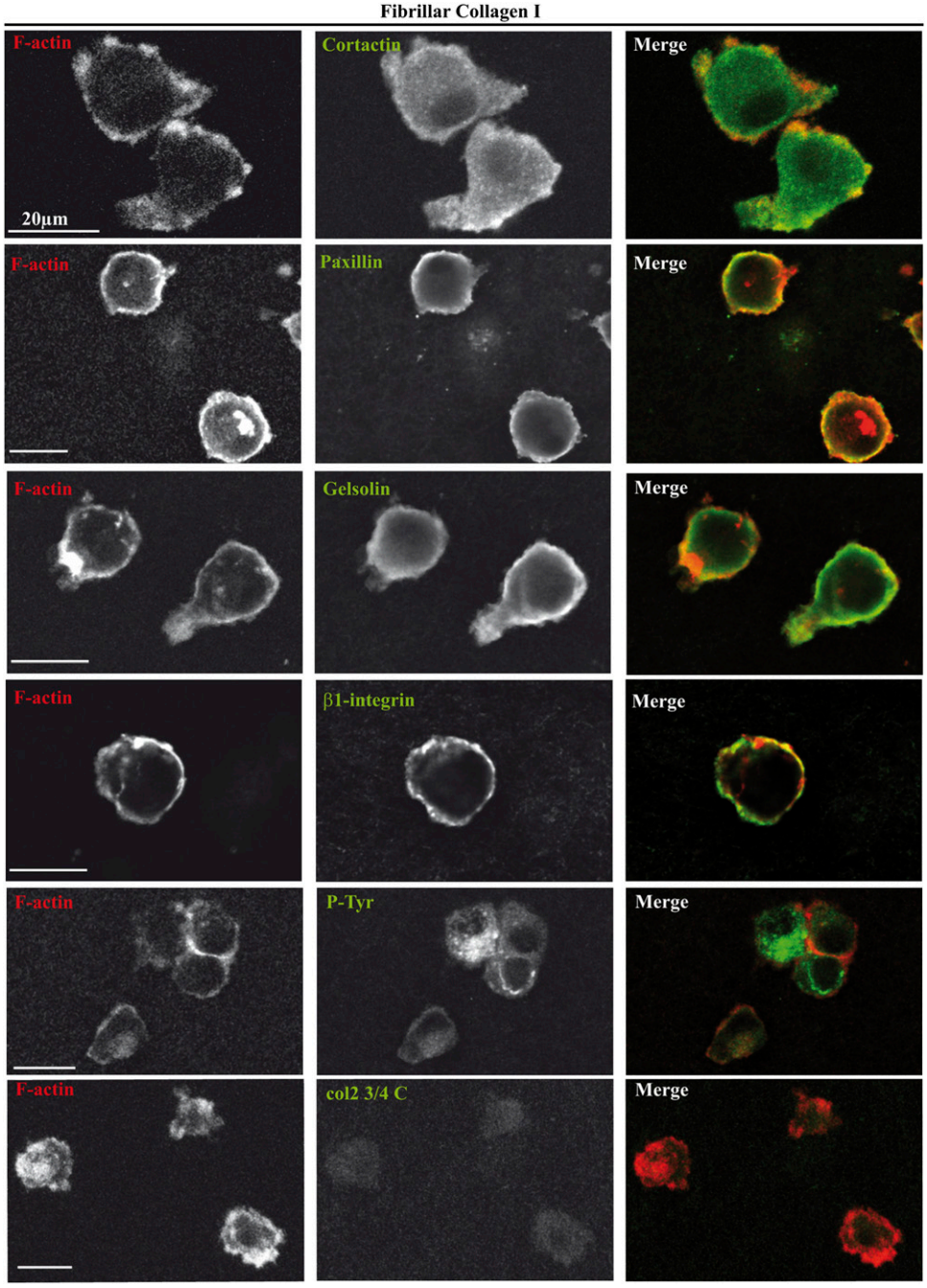

FIGURE 7. Human MDMs migrating via the amoeboid mode do not form pseudopodia enriched in F-actin, cortactin, paxillin, gelsolin, β_1-integrin, and P-tyr and do not have a collagenolytic activity. After migration in fibrillar collagen I matrices in Transwell inserts for 48–72 h, samples were fixed, permeabilized, and stained with indicated primary Abs as described in Fig. 6 and Texas Red phalloidin (original magnification ×100). Bars: 20 μm.

to sense the architecture of matrices. It is likely that adhesion receptors have distinct spatial arrangements when macrophages are in contact with collagen I organized as fibrils or as a gel. As recently reviewed, ligand spacing play a key role in environmental sensing and signaling transduction (59) with downstream signals that might differ and, in our experimental conditions, promote either amoeboid or mesenchymal migration.

As reported for endothelial and cancer cells (38, 39), we observed that macrophages can generate a persistent tunnel when they perform mesenchymal migration in Matrigel. Actually

had turned over during the time of the experiment. Note that podosomes often accumulate at the leading edge of the migrating cells. Bars: 10 μm. *B*, Human MDMs in 3D form F-actin–, cortactin-, paxillin-, gelsolin, β_1-integrin ,and P-tyr–enriched structures with collagenolytic activity at the tip of pseudopodia when migrating via the mesenchymal mode. After migration in gelled collagen I matrices in Transwell inserts for 72 h, samples were fixed, permeabilized, and stained with anticortactin, antipaxillin, antigelsolin, anti–β_1-integrin, anti–P-tyr, or $Col2_{3/4}$Cshort Abs (to detect positive collagenolytic activity) and Texas Red phalloidin. Membrane protrusions enriched in F-actin, cortactin, paxillin, gelsolin, β_1-integrin, and P-tyr and positive for collagenolytic activity are shown (*B*, arrows and *inset*). Samples were monitored by confocal microscopy (Leica SP2). Images show projections of 2–10 z-sections of 0.4 μm in depth. Bars: 20 μm. Insets in *B* are zoomed four times.

macrophage mesenchymal migration consists in two types of movement: the "slow" movement, which could be made by a leading cell, is unidirectional, proteolytic, and forms a tunnel inside the matrix. The "fast" movement consists in back and forth migration performed by the leading cell itself or by following cells. Tunnel formation might facilitate the progression of following cells through anatomic barriers. In addition, we show that mesenchymal migration, which is a protease-dependent process, is accompanied by the formation of F-actin–rich protrusions with a collagenolytic activity. In contrast, macrophage amoeboid migration, which is a protease-independent process, is not associated with membrane protrusions or collagenolytic activity.

In two dimensions, macrophages and macrophage-derived cells are the only cells to be constitutively equipped with particular adhesion structures called podosomes, exhibiting ECM proteolytic activity (44). In contrast to invadopodia, the tumor cell counterpart of podosomes (48), we observed that podosome formation in human MDMs is not affected by protease inhibitors, further supporting previous observations that podosomes and invadopodia are distinct although related structures (47). Podosomes have been studied in two dimensions and found to reorganize as a sealing zone delimitating the bone resorbing compartment of osteoclasts. The role of podosomes in macrophages is not clear yet. It is likely that when macrophages are seeded on matrices, podosomes could function as mechanosensor by analogy to results obtained in model cells forming podosome rosettes (60, 61), but the role of a proteolytic activity in this process is not obvious. In the light of our results showing that markers of podosome (such as cortactin, paxillin, gelsolin, and β_1-integrin) and a collagenolytic activity are present at the tips of 3D protrusions, we propose that podosomes could be reorganized to form these protrusive structures once macrophages infiltrate 3D matrices in a mesenchymal mode. Thus podosomes could play a central role in facilitating macrophage migration through matrices that trigger the protease-dependent migratory mode. Also cancer cells migrating inside a matrix form lateral spikes with proteolytic activity (34). On one hand, several cancer cell lines are equipped with invadopodia (46). On the other hand, it has been recently proposed that proteolytic protrusions in 3D-migrating cancer cells are related to 2D lamellipodia formed at the leading edge, which often generate proteolysis underneath the anterior rim (34). Interestingly, in macrophages migrating in two dimensions, podosomes are polarized at the leading edge lamellipodia (Ref. 44; Fig. 6, Supplemental Fig. 3). Although a lot of work remains to be done, it is tempting to propose that, in macrophages, 2D podosomes could be at the origin of 3D collagenolytic protrusions. Similarly, 3D cell adhesions have been shown to differ in organization, localization, and function from those classically described in two dimensions (62).

When cancer cell 3D migration is protease dependent, it is mostly because of MMPs (16, 34). Actually, 3D migration of cancer cells is almost entirely reliant on MMP14 (MT1-MMP) (16). However, the involvement of MMPs in macrophage migration is less clear. In vivo, MMP13 and MMP14 (MT1-MMP) are not involved in macrophage recruitment in experimental atherosclerosis (24, 25), and macrophage infiltration was unaffected by MT1-MMP deletion in an aortic aneurysm model (26). In contrast, MMP9 is playing a role in peritonitis-induced macrophage recruitment (23), but in vitro, *Mmp9*$^{-/-}$ macrophages do not exhibit any migration defect in Matrigel (23). Furthermore, we report that MMP inhibitors did not inhibit macrophage mesenchymal migration, suggesting that MMP activity is not sufficient to allow mesenchymal migration of MDMs. If we consider that MMPs are not mandatory for protease-dependent macrophage 3D migration and that a mix of protease inhibitors dedicated to cysteine-, glutamic-, and serine-proteases affects macrophage migration, we propose that proteases mostly of lysosomal origin could be implicated. Actually, the lysosomal enzyme Cathepsin B has been shown to participate in matrix invasion of transformed fibroblasts (63).

Similarly to osteoclasts, which secrete lysosomal enzymes into the podosome-derived sealing zone (64), we and others have previously shown that lysosomes play a role in the formation and organization of podosomal structures in two dimensions (63, 65). Therefore, delivery of lysosomal proteases at the level of the 3D collagenolytic structures could participate, potentially with proteases of other origins, in localized matrix degradation necessary to allow macrophage migration through a matrix structured as a dense gel. Protease identification represents a challenge because their inhibition could target macrophage mesenchymal migration without inhibiting macrophage or lymphocyte amoeboid migration. However, we keep in mind that, in the complex and various in vivo matrix environments infiltrated by macrophages under distinct pathological contexts, the role of proteases has to be dissected.

In conclusion, human macrophages have the double capacity to perform amoeboid and mesenchymal migration, which should allow these cells to migrate through all the anatomic boundaries found in the body. As they adapt their migration mode according to the matrix architecture, they probably optimize tissue infiltration without mandatory proteolysis of interstitial tissues. The pharmacological targeting of macrophage migration-related molecules for development of new anti-inflammatory and antitumor-based drug is a promising approach and this study constitutes a critical step for future works in this field.

Acknowledgments

We thank Dr. M-C. Prévost for access to the Ultrastructural Microscopy Platform of Institut Pasteur (Paris, France), the Toulouse RIO imaging platform, Juliette Fitreman for advices with rheology experiments, and Stephen J Weiss for providing BB-2516 and BB-94.

Disclosures

The authors have no financial conflicts of interest.

References

1. Yiangou, Y., P. Facer, P. Durrenberger, I. P. Chessell, A. Naylor, C. Bountra, R. R. Banati, and P. Anand. 2006. COX-2, CB2 and P2X7-immunoreactivities are increased in activated microglial cells/macrophages of multiple sclerosis and amyotrophic lateral sclerosis spinal cord. *BMC Neurol.* 6: 12–26.
2. Condeelis, J., and J. W. Pollard. 2006. Macrophages: obligate partners for tumor cell migration, invasion, and metastasis. *Cell* 124: 263–266.
3. Friedl, P., and B. Weigelin. 2008. Interstitial leukocyte migration and immune function. *Nat. Immunol.* 9: 960–969.
4. Mackay, C. R. 2008. Moving targets: cell migration inhibitors as new anti-inflammatory therapies. *Nat. Immunol.* 9: 988–998.
5. von Andrian, U. H., and C. R. Mackay. 2000. T-cell function and migration. Two sides of the same coin. *N. Engl. J. Med.* 343: 1020–1034.
6. Ley, K., C. Laudanna, M. I. Cybulsky, and S. Nourshargh. 2007. Getting to the site of inflammation: the leukocyte adhesion cascade updated. *Nat. Rev. Immunol.* 7: 678–689.
7. Kalluri, R. 2003. Basement membranes: structure, assembly and role in tumour angiogenesis. *Nat. Rev. Cancer* 3: 422–433.
8. Schindler, M., A. Nur-E-Kamal, I. Ahmed, J. Kamal, H. Y. Liu, N. Amor, A. S. Ponery, D. P. Crockett, T. H. Grafe, H. Y. Chung, et al. 2006. Living in three dimensions: 3D nanostructured environments for cell culture and regenerative medicine. *Cell Biochem. Biophys.* 45: 215–227.
9. Even-Ram, S., and K. M. Yamada. 2005. Cell migration in 3D matrix. *Curr. Opin. Cell Biol.* 17: 524–532.
10. Butcher, E. C. 1991. Leukocyte-endothelial cell recognition: three (or more) steps to specificity and diversity. *Cell* 67: 1033–1036.
11. Springer, T. A. 1994. Traffic signals for lymphocyte recirculation and leukocyte emigration: the multistep paradigm. *Cell* 76: 301–314.
12. Hooper, S., J. F. Marshall, and E. Sahai. 2006. Tumor cell migration in three dimensions. *Methods Enzymol.* 406: 625–643.
13. Doyle, A. D., F. W. Wang, K. Matsumoto, and K. M. Yamada. 2009. One-dimensional topography underlies three-dimensional fibrillar cell migration. *J. Cell Biol.* 184: 481–490.
14. Sahai, E. 2005. Mechanisms of cancer cell invasion. *Curr. Opin. Genet. Dev.* 15: 87–96.

15. Wolf, K., and P. Friedl. 2006. Molecular mechanisms of cancer cell invasion and plasticity. *Br. J. Dermatol.* 154(Suppl. 1): 11–15.
16. Sabeh, F., R. Shimizu-Hirota, and S. J. Weiss. 2009. Protease-dependent versus -independent cancer cell invasion programs: three-dimensional amoeboid movement revisited. *J. Cell Biol.* 185: 11–19.
17. Sahai, E., and C. J. Marshall. 2003. Differing modes of tumour cell invasion have distinct requirements for Rho/ROCK signalling and extracellular proteolysis. *Nat. Cell Biol.* 5: 711–719.
18. Carragher, N. O., S. M. Walker, L. A. Scott Carragher, F. Harris, T. K. Sawyer, V. G. Brunton, B. W. Ozanne, and M. C. Frame. 2006. Calpain 2 and Src dependence distinguishes mesenchymal and amoeboid modes of tumour cell invasion: a link to integrin function. *Oncogene* 25: 5726–5740.
19. Larsen, M., V. V. Artym, J. A. Green, and K. M. Yamada. 2006. The matrix reorganized: extracellular matrix remodeling and integrin signaling. *Curr. Opin. Cell Biol.* 18: 463–471.
20. Wolf, K., I. Mazo, H. Leung, K. Engelke, U. H. von Andrian, E. I. Deryugina, A. Y. Strongin, E. B. Bröcker, and P. Friedl. 2003. Compensation mechanism in tumor cell migration: mesenchymal-amoeboid transition after blocking of pericellular proteolysis. *J. Cell Biol.* 160: 267–277.
21. Sanz-Moreno, V., G. Gadea, J. Ahn, H. Paterson, P. Marra, S. Pinner, E. Sahai, and C. J. Marshall. 2008. Rac activation and inactivation control plasticity of tumor cell movement. *Cell* 135: 510–523.
22. Wolf, K., R. Müller, S. Borgmann, E. B. Bröcker, and P. Friedl. 2003. Amoeboid shape change and contact guidance: T-lymphocyte crawling through fibrillar collagen is independent of matrix remodeling by MMPs and other proteases. *Blood* 102: 3262–3269.
23. Gong, Y., E. Hart, A. Shchurin, and J. Hoover-Plow. 2008. Inflammatory macrophage migration requires MMP-9 activation by plasminogen in mice. *J. Clin. Invest.* 118: 3012–3024.
24. Deguchi, J. O., E. Aikawa, P. Libby, J. R. Vachon, M. Inada, S. M. Krane, P. Whittaker, and M. Aikawa. 2005. Matrix metalloproteinase-13/collagenase-3 deletion promotes collagen accumulation and organization in mouse atherosclerotic plaques. *Circulation* 112: 2708–2715.
25. Schneider, F., G. K. Sukhova, M. Aikawa, J. Canner, N. Gerdes, S. M. Tang, G. P. Shi, S. S. Apte, and P. Libby. 2008. Matrix-metalloproteinase-14 deficiency in bone-marrow-derived cells promotes collagen accumulation in mouse atherosclerotic plaques. *Circulation* 117: 931–939.
26. Xiong, W., R. Knispel, J. MacTaggart, T. C. Greiner, S. J. Weiss, and B. T. Baxter. 2009. Membrane-type 1 matrix metalloproteinase regulates macrophage-dependent elastolytic activity and aneurysm formation in vivo. *J. Biol. Chem.* 284: 1765–1771.
27. Tomlinson, M. L., C. Garcia-Morales, M. Abu-Elmagd, and G. N. Wheeler. 2008. Three matrix metalloproteinases are required in vivo for macrophage migration during embryonic development. *Mech. Dev.* 125: 1059–1070.
28. Zhang, Y., X. T. Bai, K. Y. Zhu, Y. Jin, M. Deng, H. Y. Le, Y. F. Fu, Y. Chen, J. Zhu, A. T. Look, et al. 2008. In vivo interstitial migration of primitive macrophages mediated by JNK-matrix metalloproteinase 13 signaling in response to acute injury. *J. Immunol.* 181: 2155–2164.
29. Sakamoto, T., and M. Seiki. 2009. Cytoplasmic tail of MT1-MMP regulates macrophage motility independently from its protease activity. *Genes Cells* 14: 617–626.
30. Astarie-Dequeker, C., E. N. N'Diaye, V. Le Cabec, M. G. Rittig, J. Prandi, and I. Maridonneau-Parini. 1999. The mannose receptor mediates uptake of pathogenic and nonpathogenic mycobacteria and bypasses bactericidal responses in human macrophages. *Infect. Immun.* 67: 469–477.
31. Zaman, M. H., L. M. Trapani, A. L. Sieminski, D. Mackellar, H. Gong, R. D. Kamm, A. Wells, D. A. Lauffenburger, and P. Matsudaira. 2006. Migration of tumor cells in 3D matrices is governed by matrix stiffness along with cell-matrix adhesion and proteolysis. *Proc. Natl. Acad. Sci. USA* 103: 10889–10894.
32. Lizárraga, F., R. Poincloux, M. Romao, G. Montagnac, G. Le Dez, I. Bonne, G. Rigaill, G. Raposo, and P. Chavrier. 2009. Diaphanous-related formins are required for invadopodia formation and invasion of breast tumor cells. *Cancer Res.* 69: 2792–2800.
33. Rossner, M., and K. M. Yamada. 2004. What's in a picture? The temptation of image manipulation. *J. Cell Biol.* 166: 11–15.
34. Wolf, K., and P. Friedl. 2009. Mapping proteolytic cancer cell-extracellular matrix interfaces. *Clin. Exp. Metastasis* 26: 289–298.
35. LeBleu, V. S., B. Macdonald, and R. Kalluri. 2007. Structure and function of basement membranes. *Exp. Biol. Med. (Maywood)* 232: 1121–1129.
36. Sabeh, F., X. Y. Li, T. L. Saunders, R. G. Rowe, and S. J. Weiss. 2009. Secreted versus membrane-anchored collagenases: relative roles in fibroblast-dependent collagenolysis and invasion. *J. Biol. Chem.* 284: 23001–23011.
37. Yoshida, D., and A. Teramoto. 2007. The use of 3-D culture in peptide hydrogel for analysis of discoidin domain receptor 1-collagen interaction. *Cell Adh. Migr.* 1: 92–98.
38. Stratman, A. N., W. B. Saunders, A. Sacharidou, W. Koh, K. E. Fisher, D. C. Zawieja, M. J. Davis, and G. E. Davis. 2009. Endothelial cell lumen and vascular guidance tunnel formation requires MT1-MMP-dependent proteolysis in 3-dimensional collagen matrices. *Blood* 114: 237–247.
39. Friedl, P., and K. Wolf. 2008. Tube travel: the role of proteases in individual and collective cancer cell invasion. *Cancer Res.* 68: 7247–7249.
40. Fackler, O. T., and R. Grosse. 2008. Cell motility through plasma membrane blebbing. *J. Cell Biol.* 181: 879–884.
41. Charras, G., and E. Paluch. 2008. Blebs lead the way: how to migrate without lamellipodia. *Nat. Rev. Mol. Cell Biol.* 9: 730–736.
42. Féréol, S., R. Fodil, B. Labat, S. Galiacy, V. M. Laurent, B. Louis, D. Isabey, and E. Planus. 2006. Sensitivity of alveolar macrophages to substrate mechanical and adhesive properties. *Cell Motil. Cytoskeleton* 63: 321–340.
43. Guarnieri, D., S. Battista, A. Borzacchiello, L. Mayol, E. De Rosa, D. R. Keene, L. Muscariello, A. Barbarisi, and P. A. Netti. 2007. Effects of fibronectin and laminin on structural, mechanical and transport properties of 3D collageneous network. *J. Mater. Sci. Mater. Med.* 18: 245–253.
44. Linder, S., and M. Aepfelbacher. 2003. Podosomes: adhesion hot-spots of invasive cells. *Trends Cell Biol.* 13: 376–385.
45. Evans, J. G., and P. Matsudaira. 2006. Structure and dynamics of macrophage podosomes. *Eur. J. Cell Biol.* 85: 145–149.
46. Buccione, R., G. Caldieri, and I. Ayala. 2009. Invadopodia: specialized tumor cell structures for the focal degradation of the extracellular matrix. *Cancer Metastasis Rev.* 28: 137–149.
47. Gimona, M., R. Buccione, S. A. Courtneidge, and S. Linder. 2008. Assembly and biological role of podosomes and invadopodia. *Curr. Opin. Cell Biol.* 20: 235–241.
48. Clark, E. S., A. S. Whigham, W. G. Yarbrough, and A. M. Weaver. 2007. Cortactin is an essential regulator of matrix metalloproteinase secretion and extracellular matrix degradation in invadopodia. *Cancer Res.* 67: 4227–4235.
49. Discher, D. E., P. Janmey, and Y. L. Wang. 2005. Tissue cells feel and respond to the stiffness of their substrate. *Science* 310: 1139–1143.
50. Berrier, A. L., and K. M. Yamada. 2007. Cell-matrix adhesion. *J. Cell. Physiol.* 213: 565–573.
51. Bowden, E. T., E. Onikoyi, R. Slack, A. Myoui, T. Yoneda, K. M. Yamada, and S. C. Mueller. 2006. Co-localization of cortactin and phosphotyrosine identifies active invadopodia in human breast cancer cells. *Exp. Cell Res.* 312: 1240–1253.
52. Spinardi, L., and P. C. Marchisio. 2006. Podosomes as smart regulators of cellular adhesion. *Eur. J. Cell Biol.* 85: 191–194.
53. Block, M. R., C. Badowski, A. Millon-Fremillon, D. Bouvard, A. P. Bouin, E. Faurobert, D. Gerber-Scokaert, E. Planus, and C. Albiges-Rizo. 2008. Podosome-type adhesions and focal adhesions, so alike yet so different. *Eur. J. Cell Biol.* 87: 491–506.
54. Abram, C. L., and C. A. Lowell. 2009. The ins and outs of leukocyte integrin signaling. *Annu. Rev. Immunol.* 27: 339–362.
55. Brockbank, E. C., J. Bridges, C. J. Marshall, and E. Sahai. 2005. Integrin β_1 is required for the invasive behaviour but not proliferation of squamous cell carcinoma cells in vivo. *Br. J. Cancer* 92: 102–112.
56. Friedl, P., and K. Wolf. 2009. Proteolytic interstitial cell migration: a five-step process. *Cancer Metastasis Rev.* 28: 129–135.
57. Lämmermann, T., B. L. Bader, S. J. Monkley, T. Worbs, R. Wedlich-Söldner, K. Hirsch, M. Keller, R. Förster, D. R. Critchley, R. Fässler, and M. Sixt. 2008. Rapid leukocyte migration by integrin-independent flowing and squeezing. *Nature* 453: 51–55.
58. Denys, H., G. Braems, K. Lambein, P. Pauwels, A. Hendrix, A. De Boeck, V. Mathieu, M. Bracke, and O. De Wever. 2009. The extracellular matrix regulates cancer progression and therapy response: implications for prognosis and treatment. *Curr. Pharm. Des.* 15: 1373–1384.
59. Geiger, B., J. P. Spatz, and A. D. Bershadsky. 2009. Environmental sensing through focal adhesions. *Nat. Rev. Mol. Cell Biol.* 10: 21–33.
60. Collin, O., P. Tracqui, A. Stephanou, Y. Usson, J. Clément-Lacroix, and E. Planus. 2006. Spatiotemporal dynamics of actin-rich adhesion microdomains: influence of substrate flexibility. *J. Cell Sci.* 119: 1914–1925.
61. Collin, O., S. Na, F. Chowdhury, M. Hong, M. E. Shin, F. Wang, and N. Wang. 2008. Self-organized podosomes are dynamic mechanosensors. *Curr. Biol.* 18: 1288–1294.
62. Cukierman, E., R. Pankov, D. R. Stevens, and K. M. Yamada. 2001. Taking cell-matrix adhesions to the third dimension. *Science* 294: 1708–1712.
63. Tu, C., C. F. Ortega-Cava, G. Chen, N. D. Fernandes, D. Cavallo-Medved, B. F. Sloane, V. Band, and H. Band. 2008. Lysosomal cathepsin B participates in the podosome-mediated extracellular matrix degradation and invasion via secreted lysosomes in v-Src fibroblasts. *Cancer Res.* 68: 9147–9156.
64. Baron, R. 1989. Polarity and membrane transport in osteoclasts. *Connect. Tissue Res.* 20: 109–120.
65. Cougoule, C., S. Carréno, J. Castandet, A. Labrousse, C. Astarie-Dequeker, R. Poincloux, V. Le Cabec, and I. Maridonneau-Parini. 2005. Activation of the lysosome-associated p61Hck isoform triggers the biogenesis of podosomes. *Traffic* 6: 682–694.